O.V. Smitiukh, I.I. Petrus'

The Phase Equilibrium in the HgS–Ga$_2$S$_3$–Bi(Sb)$_2$S$_3$ Systems

Lesya Ukrainka Volyn National University, Department of Chemistry and Technology, Lutsk, Ukraine,
Smitiukh.Oleksandr@vnu.edu.ua

Phase equilibria in the quasi-ternary systems HgS–Ga$_2$S$_3$–Bi(Sb)$_2$S$_3$ were studied by physico-chemical analysis methods on 177 alloys that were synthesized by direct single-temperature method. Phase diagrams of the quasi-binary systems HgS–Bi$_2$S$_3$ and Ga$_2$S$_3$–Bi$_2$S$_3$, six vertical sections (HgGa$_2$S$_4$–HgBi$_2$S$_4$, HgGa$_2$S$_4$–Bi$_2$S$_3$, HgGa$_6$S$_{10}$–Bi$_2$S$_3$, HgGa$_6$S$_{10}$–HgBi$_2$S$_4$, HgGa$_2$S$_4$–Sb$_2$S$_3$, and HgS–"GaSbS$_3$"), and liquidus surface projections were investigated. Due to large primary crystallization region of mercury thiogallate, particularly at the HgGa$_2$S$_4$–Bi$_2$S$_3$ and HgGa$_2$S$_4$–HgBi$_2$S$_4$ sections, and low temperature (950-1050 K), the growth of single crystals of mercury thiogallate is possible using solution-melt method.

Keywords: phase diagram, solidus, quasi-binary system, liquidus surface projection.

Received 03 July 2023; Accepted 8 September 2023.

Introduction

According to the literary information, HgGa$_2$S$_4$ is one of the best non-linear optical materials for parametric light generators for the middle IR region of the electromagnetic spectrum with high laser damage threshold [1]. Single crystals of the compound were obtained by CVD [2] or from solution using near-stoichiometric compositions [3] due to incongruent melting of mercury thiogalate at 1159 K. However, the using of such compositions is problematic due to high vapor pressure of HgS. The solution-melt growth method may be the answer. The alloys of the HgS–Ga$_2$S$_3$–Bi(Sb)$_2$S$_3$ systems may be used as a solvent but the selection of the growth conditions requires specific data on the phase diagrams of the system.

Binary system components HgS, Ga$_2$S$_3$, Bi$_2$S$_3$ and Sb$_2$S$_3$ melt congruently at 1093 K [4], 1383 K [5], 1048 K [6], and 823 K [7] respectively, and have narrow homogeneity regions near the stoichiometric composition.

The crystal structure of HgBi$_2$S$_4$ has an order-disorder character and consists of (001) layers, which are built up

Table 1.

The crystallographic data on binary and ternary compounds

Compound	Space group	Lattice parameters, nm			Ref.
		a	*b*	*c*	
α'-HgS	P3$_1$21	0.4136	-	0.9501	[7]
α-HgS	F-43m	0.585	-	-	[7]
α-Ga$_2$S$_3$	F-43m	0.517	-	-	[7]
β-Ga$_2$S$_3$	P6$_3$mc	0.3685	-	0.6018	[7]
γ-Ga$_2$S$_3$	P6$_5$	0.638	-	0.809	[7]
Bi$_2$S$_3$	Pnma	1.1154	1.1288	0.3985	[8]
Sb$_2$S$_3$	Pnma	1.1311	0.3836	1.1229	[9,10]
HgBi$_2$S$_4$	C2/m	1.417	0.406 β = 118.27°	1.399	[11]
HgGa$_2$S$_4$	I-4	0.55106	0.55106	1.02392	[12]

by Bi_2S_4 rods of edge-sharing square-pyramidal $[BiS_5]$ polyhedra [13]. Such a layered-like structure usually can cause special properties. The films of the $MnSb_2S_4$ phase (structure type of $HgBi_2S_4$) films demonstrate a direct optical transition with variable energy gap values (1.77–1.53 eV). They behave as p-type semiconductors [14]. According to the work [15], a high thermoelectric efficiency (for the $HgGa_2S_4$ phase) can be achieved through controlling the carrier concentration and pressure. High figure of merit of 0.98 was obtained for the p-type $HgGa_2S_4$ chalcopyrite. The materials based on the $HgGa_2S_4$ phase can find application as no polarized radiation photodetectors [16]. To find an effective method of obtaining the $HgBi_2S_4$ and $HgGa_2S_4$ phases are important issue of the work.

Quasi-binary systems
HgS–Ga$_2$S$_3$

The HgS–Ga_2S_3 phase diagram belongs to the peritectic type [17]. Two ternary compounds are formed in the system, $HgGa_6S_{10}$ (endothermic, incongruent, melts at 1235 K) and $HgGa_2S_4$ [18] (peritectic, melts at 1159 K).
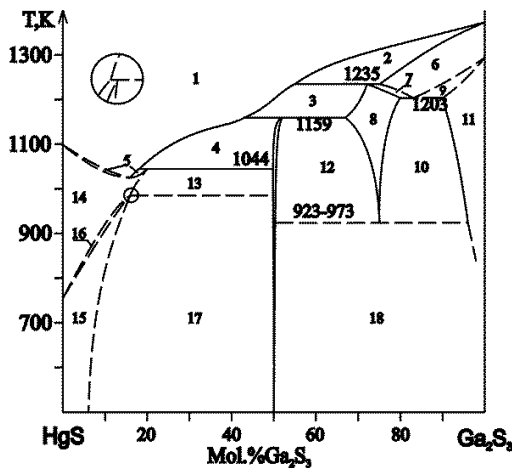

Fig. 1. Phase diagram of the HgS–Ga_2S_3 system [17]:
1 – L, 2 – L+ β-Ga_2S_3, 3 – L+$HgGa_6S_{10}$, 4 – L+$HgGa_2S_4$,
5 – L+α, 6 – β-Ga_2S_3, 7 – $HgGa_6S_{10}$+ β-Ga_2S_3,
8 – $HgGa_6S_{10}$, 9 – β-Ga_2S_3+ β'-Ga_2S_3, 10 – $HgGa_6S_{10}$+ β'-Ga_2S_3, 11 – β'-Ga_2S_3, 12 – $HgGa_2S_4$+$HgGa_6S_{10}$,
13 – α+$HgGa_2S_4$, 14 – α, 15 – δ, 16 – α+δ,
17 – δ+$HgGa_2S_4$, 18 – $HgGa_2S_4$+ β'-Ga_2S_3.

HgS–Bi$_2$S$_3$

The HgS–Bi_2S_3 phase diagram belongs to the eutectic type [19]. The horizontal line at 628 K corresponds to the polymorphous transformation α-HgS↔α'-HgS. The formation of the $HgBi_2S_4$ compound is reported in [20] (monoclinic S.G. $C2/m$, a=14.175 Å, b=4.0563 Å, c=13.983 Å, β=118,19(3)°), but that is not reflected in the diagram in [19].

HgS–Sb$_2$S$_3$

The HgS–Sb_2S_3 phase diagram belongs to the eutectic type [19], with the eutectic point coordinates 53 mol.% Sb_2S_3 and 735 K. The temperature of the polymorphous transformation of HgS (618 K) does not depend on the content of Sb_2S_3 that indicates the absence of solid solubility in HgS.

Ga$_2$S$_3$–Bi$_2$S$_3$

The Ga_2S_3–Bi_2S_3 system features the $BiGa_9S_{15}$ compound that forms incongruently in the reaction $L+Ga_2S_3 \Leftrightarrow BiGa_9S_{15}$ and melts at 723 K [21]. The coordinates of the eutectic point are 888 K and 40 mol.% Ga_2S_3.

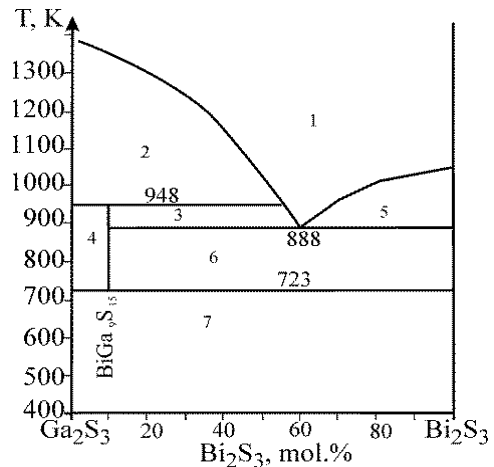**Fig. 2.** Phase diagram of the Ga_2S_3–Bi_2S_3 system [21]:
1 – L, 2 – L+ Ga_2S_3, 3 – L+$BiGa_9S_{15}$; 4 – Ga_2S_3+$BiGa_9S_{15}$,
5 – L+Bi_2S_3, 6 – $BiGa_9S_{15}$+Bi_2S_3, 7 – Ga_2S_3+Bi_2S_3.

Ga$_2$S$_3$–Sb$_2$S$_3$

The Ga_2S_3–Sb_2S_3 phase diagram belongs to the eutectic type [22]. The eutectic point coordinates are 80 mol.% Sb_2S_3 and 733 K.

Several discrepancies concerning quasi-binary side systems were the reason for the re-investigation of HgS–Bi_2S_3, Ga_2S_3–Bi_2S_3, and Ga_2S_3–Sb_2S_3 phase diagrams. Additionally, four vertical sections of the HgS–Ga_2S_3–Bi_2S_3 system and two sections of the HgS–Ga_2S_3–Sb_2S_3 system were investigated in this work.

I. Experimental

The compounds and alloys of the studied systems were synthesized from semiconductor-purity elements (Ga, Bi, Sb and S) and pre-synthesized HgS. The calculated amounts of starting components were loaded into quartz ampoules that were evacuated to residual pressure of 10^{-2} Pa and soldered. Based on the p-T diagrams of the starting materials, single-temperature method was selected for the synthesis of alloys. The synthesis was performed in commercial programmable furnaces. At the first stage of synthesis, we heated ampoules with substances in the flame of an oxygen-gas burner until elemental sulfur is completely bound. As follows, the components that would create a lot of pressure were absent. Additionally, the quartz ampoules were covered with asbestos cord and then, the ampoules were placed in commercial programmable furnaces. The temperature was raised at the rate of 20–30 K/h to the maximum of 1120-1320 K, with 4 h stays at the melting points of the batch components. The alloys were then cooled at the rate of 10–20 K/h to 670 K where homogenizing annealing was held for 500 h. Annealed alloys were quenched into 25% aqueous NaCl solution.

Differential thermal analysis utilized a Paulik–

Paulik–Erdei derivatograph, with Pt/Pt-Rh thermocouple and Al$_2$O$_3$ as a standard. All static parameters were stable during the experiment. X-ray phase analysis using WinCSD software package [23] was performed on diffraction patterns recorded at a DRON 4-13 diffractometer (CuKα radiation). Dashed or dotted part of lines in the diagrams were plotted theoretically because during the experiment, we could not register the thermodynamic effect)

II. Results and discussion

2.1. Quasi-ternary system HgS–Ga$_2$S$_3$–Bi$_2$S$_3$
2.1.1. Quasi-binary system HgS–Bi$_2$S$_3$

Since the existence of the HgBi$_2$S$_4$ compound was not reflected in the phase diagram [10], the HgS–Bi$_2$S$_3$ quasi-binary system was re-investigated. As a result, it was confirmed that the compound HgBi$_2$S$_4$ is formed in the system. The phase diagram belongs to the eutectic type.
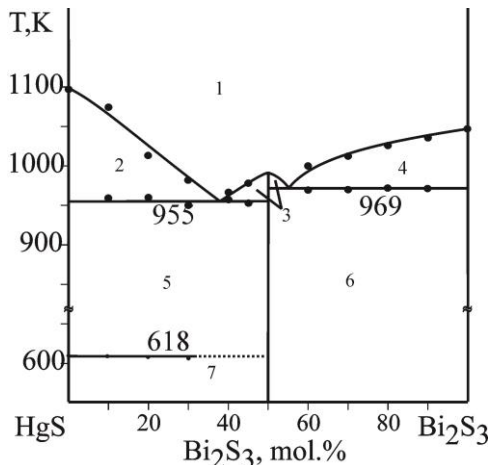

Fig. 3. Phase diagram of the HgS–Bi$_2$S$_3$ system: 1 – L, 2 – L + α-HgS, 3 – L + HgBi$_2$S$_4$, 4 – L + Bi$_2$S$_3$, 5 – α-HgS + HgBi$_2$S$_4$, 6 – HgBi$_2$S$_4$ + Bi$_2$S$_3$, 7 – α'- HgS+HgBi$_2$S$_4$ (α-HgS – sphalerite, α'- HgS – cinnabar) (a line at 628 K is polymorphic transition of HgS;).

The system liquidus consists of three fields of the primary crystallization of HgS, HgBi$_2$S$_4$, and Bi$_2$S$_3$. The interaction of HgBi$_2$S$_4$ and other system components is eutectic. The system features two eutectic reactions, L$\leftrightarrow\alpha$-HgS(sphalerite) + HgBi$_2$S$_4$ (eutectic coordinates 955 K and 38 mol.% Bi$_2$S$_3$) and L$\leftrightarrow$HgBi$_2$S$_4$ + Bi$_2$S$_3$ (969 K, 55 mol.% Bi$_2$S$_3$). The horizontal line at 618 K reflects the polymorphous transformation α-HgS$\leftrightarrow$ α'- HgS.

2.1.2. Quasi-binary system Ga$_2$S$_3$–Bi$_2$S$_3$

The full-valent chalcogenides of the A$^{III}_2$B$^{VI}_3$ composition (A^{III} – Ga, In; B^{VI} – S, Se, Te) are known to have a range of polymorphous transformations that were disregarded in the Ga$_2$S$_3$– Bi$_2$S$_3$ phase diagram in [12].

The system liquidus (Fig. 4) is represented by the fields of the primary crystallization of β-solid solutions of HT-Ga$_2$S$_3$ (field 2) and β'-solid solutions of LT-Ga$_2$S$_3$ (field 6), and of Bi$_2$S$_3$ (field 7). The region of primary crystallization of β-solid solutions extends to 32 mol.%

Bi$_2$S$_3$. The metatectic reaction β-Ga$_2$S$_3\leftrightarrow$L+β'-Ga$_2$S$_3$ occurs at 1136 K. The invariant eutectic process L$\leftrightarrow$ β'-Ga$_2$S$_3$+Bi$_2$S$_3$ takes place at 909 K, the eutectic point coordinate is 65 mol.% Bi$_2$S$_3$.
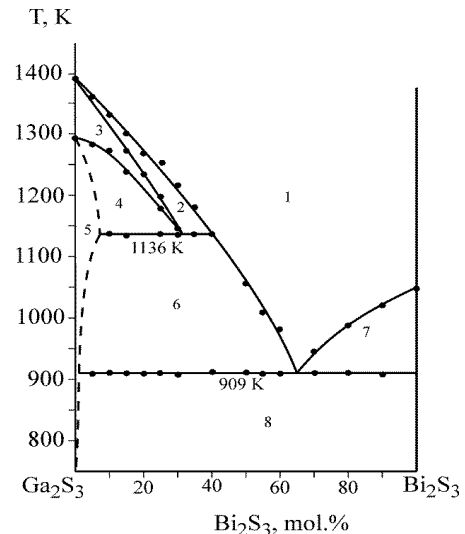
Fig. 4. Phase diagram of the Ga$_2$S$_3$–Bi$_2$S$_3$ system:
1 – L, 2 – L + β-Ga$_2$S$_3$, 3 – β-Ga$_2$S$_3$,
4 – β-Ga$_2$S$_3$ + β'-Ga$_2$S$_3$, 5 – β'-Ga$_2$S$_3$, 6 – L + β'-Ga$_2$S$_3$,
7 – L + Bi$_2$S$_3$, 8 – β'-Ga$_2$S$_3$ + Bi$_2$S$_3$.

According to [12], the BiGa$_9$S$_{15}$ compound exists in the temperature range 948–723 K. A sample of the BiGa$_9$S$_{15}$ composition was annealed at 670 K, 770 K, and 870 K. Based on X-ray phase analysis (using X'Pert High Score Plus program), the alloy is two-phase in the entire temperature range and consists of β'-Ga$_2$S$_3$ and Bi$_2$S$_3$.

2.1.3. The HgGa$_2$S$_4$–HgBi$_2$S$_4$ section ((HgS)$_{0.5}$(Ga$_2$S$_3$)$_{0.5}$–(HgS)$_{0.5}$(Bi$_2$S$_3$)$_{0.5}$)

The vertical section HgGa$_2$S$_4$–HgBi$_2$S$_4$ (Fig. 6) belongs to the eutectic type. Given the incongruent formation of mercury thiogallate, the section is quasi-binary only in the sub-solidus part. The section liquidus consists of three fields of the primary crystallization of HgGa$_6$S$_{10}$, HgGa$_2$S$_4$ and HgBi$_2$S$_4$. The crystallization of all alloys ends in the invariant eutectic process L$\leftrightarrow$HgGa$_2$S$_4$+HgBi$_2$S$_4$ at 915 K. The horizontal line at 1130 K corresponds to the binary peritectic process L + Hg.Ga$_6$S$_{10}$ $\leftrightarrow$ HgGa$_2$S$_4$.

2.1.4. The HgGa$_2$S$_4$–Bi$_2$S$_3$ section (((HgS)$_{0.5}$(Ga$_2$S$_3$)$_{0.5}$–Bi$_2$S$_3$)

Phase diagram of the HgGa$_2$S$_4$–Bi$_2$S$_3$ section (Fig. 7) is similar to the previous section.

The section liquidus consists of three fields of the primary crystallization of HgGa$_6$S$_{10}$, HgGa$_2$S$_4$ and Bi$_2$S$_3$. The section is quasi-binary only in the sub-solidus part due to incongruent type of formation of mercury thiogallate. The crystallization of all alloys ends in the binary eutectic L$\leftrightarrow$HgGa$_2$S$_4$+Bi$_2$S$_3$ at 920 K. The horizontal line at 1048 K reflects the binary peritectic process L + HgGa$_6$S$_{10}\leftrightarrow$ HgGa$_2$S$_4$.

2.1.5. The HgGa$_6$S$_{10}$–Bi$_2$S$_3$ section ((HgS)$_{0.25}$(Ga$_2$S$_3$)$_{0.75}$–Bi$_2$S$_3$)

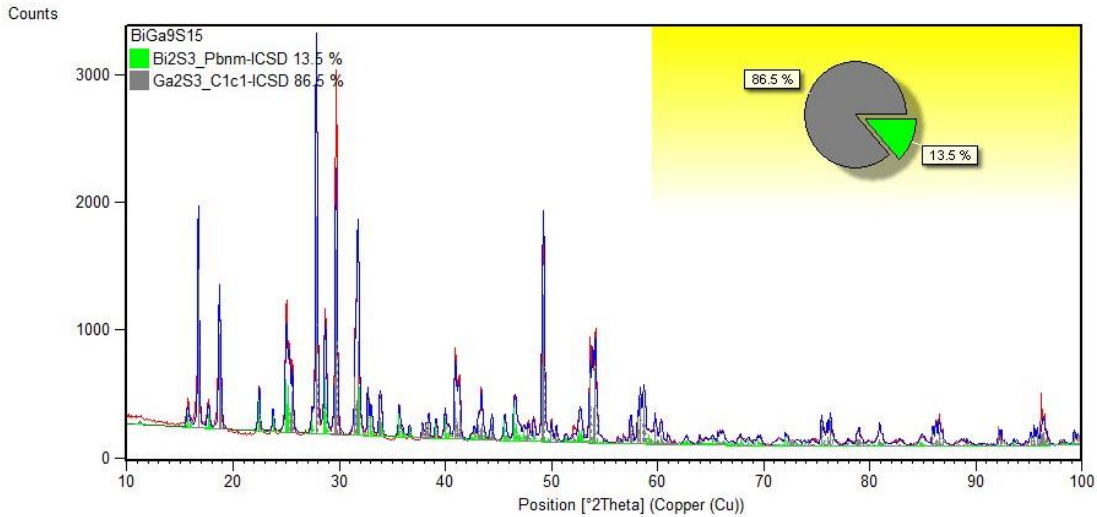The liquidus of the HgGa$_6$S$_{10}$–Bi$_2$S$_3$ section (Fig. 8) consists of three fields of the primary crystallization of

Fig. 5. Experimental diffraction pattern of the $BiGa_9S_{15}$ sample annealed at 770 K (red line) and theoretical patterns of binary compounds (green line – Bi_2S_3, blue line – β'-Ga_2S_3).
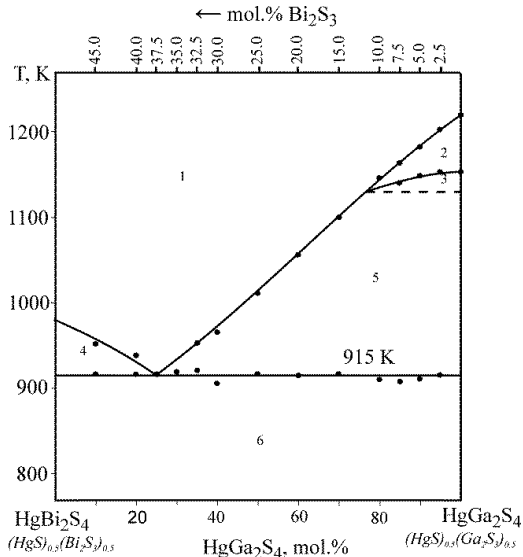

Fig. 6. Phase diagram of the $HgGa_2S_4$–$HgBi_2S_4$ system: 1 – L, 2 – L + $HgGa_6S_{10}$, 3 – L + $HgGa_6S_{10}$ + +$HgGa_2S_4$, 4 – L + $HgBi_2S_4$, 5 – L + $HgGa_2S_4$, 6 – $HgGa_2S_4$ + $HgBi_2S_4$. Hereafter, the top composition axis represents the molar fraction of one of the binary compounds from the concentration triangle. (**Table S1**. Compositions of the alloys of the $HgGa_2S_4$– $HgBi_2S_4$ section re-calculated to the concentration triangle of the quasi-ternary system HgS–Ga_2S_3–Bi_2S_3).

Fig. 7. Phase diagram of the $HgGa_2S_4$–Bi_2S_3 system: 1 – L, 2 – L + $HgGa_6S_{10}$, 3 – L + $HgGa_6S_{10}$ + +$HgGa_2S_4$, 4 – L + $HgGa_2S_4$, 5 – L + Bi_2S_3, 6 – $HgGa_2S_4$ + Bi_2S_3, (**Table S2.** Compositions of the alloys of the $HgGa_2S_4$–Bi_2S_3 section re-calculated to the concentration triangle of the quasi-ternary system HgS–Ga_2S_3–Bi_2S_3).
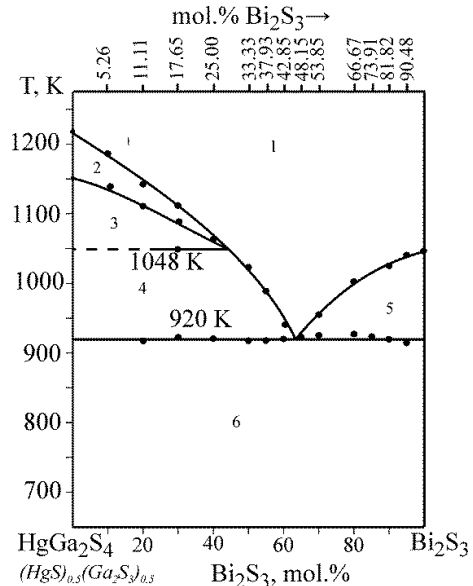
β'-Ga_2S_3, β-Ga_2S_3 and $HgBi_2S_4$. The transitional process U_1 (L + β-Ga_2S_3 ↔ $HgGa_6S_{10}$ + β'-Ga_2S_3) occurs at 1080 K and U_2 (L + $HgGa_6S_{10}$ ↔ β'-Ga_2S_3 + $HgGa_2S_4$) occurs at 1003 K. The invariant ternary eutectic process L↔ β'-Ga_2S_3 + $HgGa_2S_4$ + Bi_2S_3 at 902 K completes the crystallization of all alloys.

2.1.6. The $HgBi_2S_4$–$HgGa_6S_{10}$ section $((HgS)_{0.5}(Bi_2S_3)_{0.5}$–$(HgS)_{0.2}(Ga_2S_3)_{0.8})$

The liquidus of the $HgGa_6S_{10}$– $HgBi_2S_4$ section (Fig. 9) consists of three fields of the primary crystallization of β'-Ga_2S_3, β-Ga_2S_3 and $HgBi_2S_4$. The crystallization of almost all alloys ends in four-phase

eutectic processes L↔ β'-Ga_2S_3 + $HgGa_2S_4$ + Bi_2S_3 (902 K) and L↔ $HgBi_2S_4$ + $HgGa_2S_4$ + Bi_2S_3 (864 K). The line at ~1025 K is not invariant. The $HgGa_6S_{10}$ exists in the temperature range 1235 K – 923÷973 K (Fig.1). Below 923 K it decomposes into $HgGa_2S_4$ and β'-Ga_2S_3 (field 10). The field 8 is binary, and in the field 9, $HgGa_2S_4$ crystallizes and the field is ternary.

2.1.7. The HgS–Ga_2S_3–Bi_2S_3 section at 670 K

Phase equilibria in the quasi-ternary system HgS–Ga_2S_3–Bi_2S_3 were studied on 95 alloys, the chemical and phase composition of which is shown in Fig. 10.
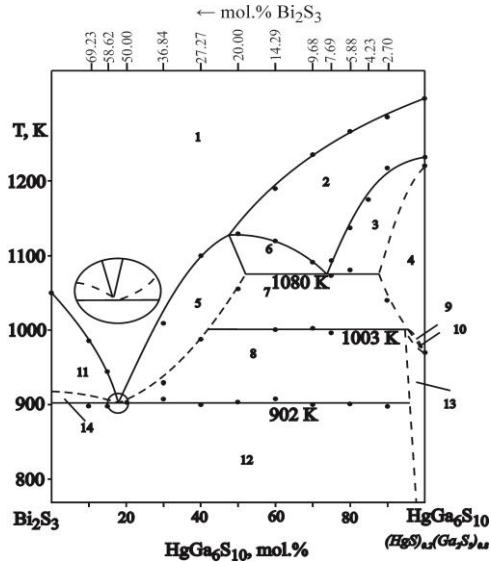
Fig. 8. Phase diagram of the HgGa$_6$S$_{10}$–Bi$_2$S$_3$ system: 1 – L, 2 – L + β-Ga$_2$S$_3$, 3 – β-Ga$_2$S$_3$ + HgGa$_6$S$_{10}$, 4 – HgGa$_6$S$_{10}$, 5 – L + β'-Ga$_2$S$_3$, 6 – L + β'-Ga$_2$S$_3$ + β-Ga$_2$S$_3$, 7 – L + β'-Ga$_2$S$_3$ + HgGa$_6$S$_{10}$, 8 – L + β'-Ga$_2$S$_3$ + HgGa$_2$S$_4$, 9 – β'-Ga$_2$S$_3$ + HgGa$_6$S$_{10}$, 10 – β'-Ga$_2$S$_3$ + HgGa$_6$S$_{10}$ + HgGa$_2$S$_4$, 11 – L + Bi$_2$S$_3$, 12 – β'-Ga$_2$S$_3$ + Bi$_2$S$_3$ + HgGa$_2$S$_4$, 13 – β'-Ga$_2$S$_3$ + +HgGa$_2$S$_4$, 14 – L + Bi$_2$S$_3$ + HgGa$_2$S$_4$, (**Table S3.** Compositions of the alloys of the HgGa$_6$S$_{10}$–Bi$_2$S$_3$ section re-calculated to the concentration triangle of the quasi-ternary system HgS–Ga$_2$S$_3$–Bi$_2$S$_3$;)
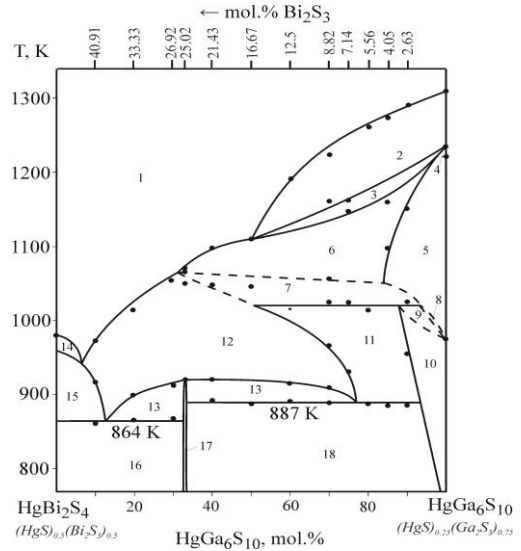

Fig. 9. Phase diagram of the *HgBi$_2$S$_4$–HgGa$_6$S$_{10}$* system: 1 – L, 2 – L + β-Ga$_2$S$_3$, 3 – L + β-Ga$_2$S$_3$ + +HgGa$_6$S$_{10}$, 4 – β-Ga$_2$S$_3$ + HgGa$_6$S$_{10}$, 5 – HgGa$_6$S$_{10}$, 6 – L + HgGa$_6$S$_{10}$, 7 – L + HgGa$_6$S$_{10}$ + HgGa$_2$S$_4$, 8 – β'-Ga$_2$S$_3$ + HgGa$_6$S$_{10}$, 9 – β'-Ga$_2$S$_3$ + HgGa$_6$S$_{10}$ + +HgGa$_2$S$_4$, 10 – β'-Ga$_2$S$_3$ + HgGa$_2$S$_4$, 11 – L + β'-Ga$_2$S$_3$ + HgGa$_2$S$_4$, 12 – L + HgGa$_2$S$_4$, 13 – L + Bi$_2$S$_3$+ +HgGa$_2$S$_4$, 14 – L + HgBi$_2$S$_4$, 15 – L + HgGa$_2$S$_4$ + +HgBi$_2$S$_4$, 16 – HgBi$_2$S$_4$ + Bi$_2$S$_3$ + HgGa$_2$S$_4$, 17 – Bi$_2$S$_3$ + HgGa$_2$S$_4$, 18 – β'-Ga$_2$S$_3$ + Bi$_2$S$_3$ + + HgGa$_2$S$_4$ (**Table S4.** Compositions of the alloys of the HgGa$_6$S$_{10}$–HgBi$_2$S$_4$ section re-calculated to the concentration triangle of the quasi-ternary system HgS–Ga$_2$S$_3$–Bi$_2$S$_3$).
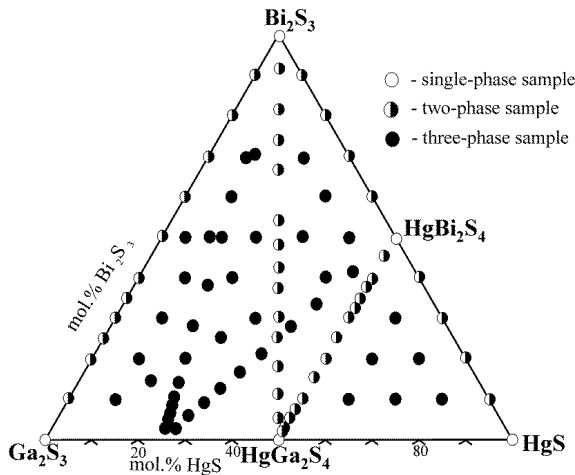

Fig. 10. The number of phases in equilibrium at 670 K.

The sections HgGa$_2$S$_4$–Bi$_2$S$_3$ and HgGa$_2$S$_4$–HgBi$_2$S$_4$ are quasi-binary only in the sub-solidus region due to incongruent type of formation of HgGa$_2$S$_4$.

2.1.8. Liquidus surface projection of the quasi-ternary system HgS–Ga$_2$S$_3$–Bi$_2$S$_3$

Liquidus surface projection of the HgS–Ga$_2$S$_3$–Bi$_2$S$_3$ system on the concentration triangle was plotted from the results presented above (Fig.10). Liquidus surface projection of the HgS–Ga$_2$S$_3$–Bi$_2$S$_3$ system onto the

concentration triangle (Fig. 11) was plotted from the results presented above. It consists of five fields of the primary crystallization of HgS, HgGa$_2$S$_4$, Bi$_2$S$_3$, HgGa$_6$S$_{10}$, HgBi$_2$S$_4$, β'-Ga$_2$S$_3$, and β-Ga$_2$S$_3$ which are separated by eleven monovariant lines and fourteen invariant points. The nature and temperature of invariant processes are summarized in Fig. 11.
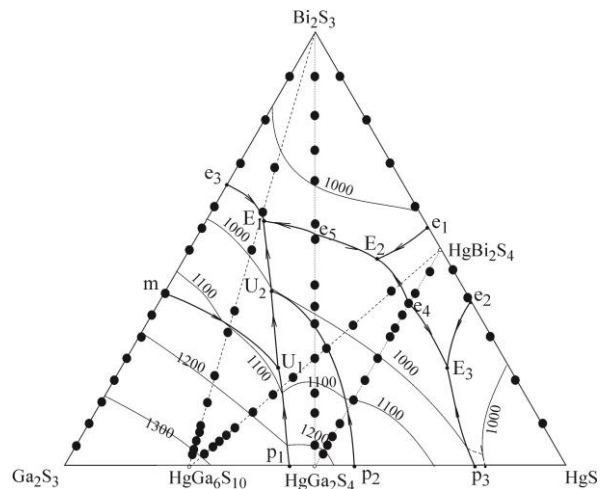

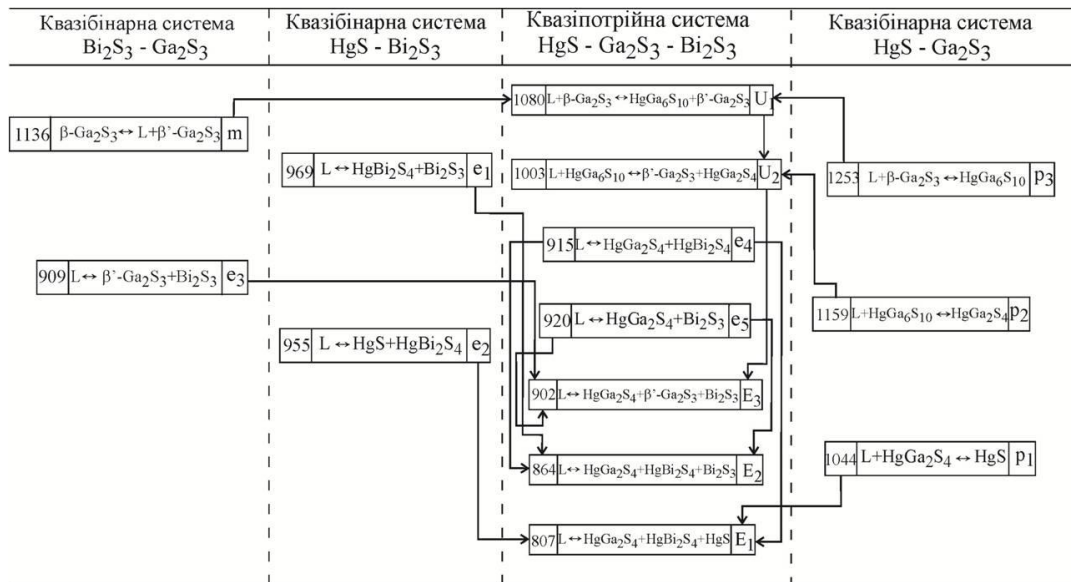**Fig. 11.** Liquidus surface projection of the quasi-ternary system *HgS–Ga$_2$S$_3$–Bi$_2$S$_3$.*

Квазібінарна система Bi$_2$S$_3$ - Ga$_2$S$_3$	Квазібінарна система HgS - Bi$_2$S$_3$	Квазіпотрійна система HgS - Ga$_2$S$_3$ - Bi$_2$S$_3$	Квазібінарна система HgS - Ga$_2$S$_3$

Fig.12. The nature and temperature of invariant processes in the HgS–Ga$_2$S$_3$–Bi$_2$S$_3$ system.

2.2. Quasi-ternary system HgS–Ga$_2$S$_3$–Sb$_2$S$_3$
2.2.1. Quasi-binary system Ga$_2$S$_3$-Sb$_2$S$_3$

Fifteen samples were synthesized to investigate the phase diagram of the Ga$_2$S$_3$–Sb$_2$S$_3$ system. The phase diagram is plotted from the results of differential thermal analysis (DTA) (Fig. 13).
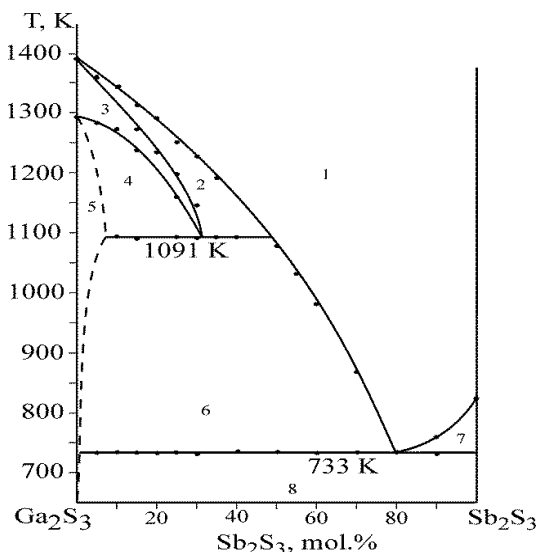

Fig. 13. Phase diagram of the Ga$_2$S$_3$–Sb$_2$S$_3$ system: 1 – L, 2 – L + β-Ga$_2$S$_3$, 3 – β-Ga$_2$S$_3$, 4 – β-Ga$_2$S$_3$ + β'-Ga$_2$S$_3$, 5 – β'-Ga$_2$S$_3$, 6 – L + β'-Ga$_2$S$_3$, 7 – L + Sb$_2$S$_3$, 8 – + β'-Ga$_2$S$_3$ + Sb$_2$S$_3$.

The system liquidus consists of fields of the primary crystallization of β -solid solutions of HT-Ga$_2$S$_3$ (field 2), β'-solid solutions of LT-Ga$_2$S$_3$ (field 6), and of Sb$_2$S$_3$ (field 7). The extent of the region of primary crystallization of γ-solid solutions reaches 52 mol.% Sb$_2$S$_3$. The invariant metatectic process β-Ga$_2$S$_3$ $\leftrightarrow$ L+ β'-Ga$_2$S$_3$ occurs at 1091 K. The eutectic process L $\leftrightarrow$ β'-Ga$_2$S$_3$+Sb$_2$S$_3$ take place at 733 K. The eutectic point corresponds to 80 mol.% Sb$_2$S$_3$.

2.2.2. The HgGa$_2$S$_4$–Sb$_2$S$_3$ section ((HgS)$_{0.5}$(Ga$_2$S$_3$)$_{0.5}$–Sb$_2$S$_3$)

The HgGa$_2$S$_4$–Sb$_2$S$_3$ phase diagram plotted from DTA results is shown in Fig. 14.
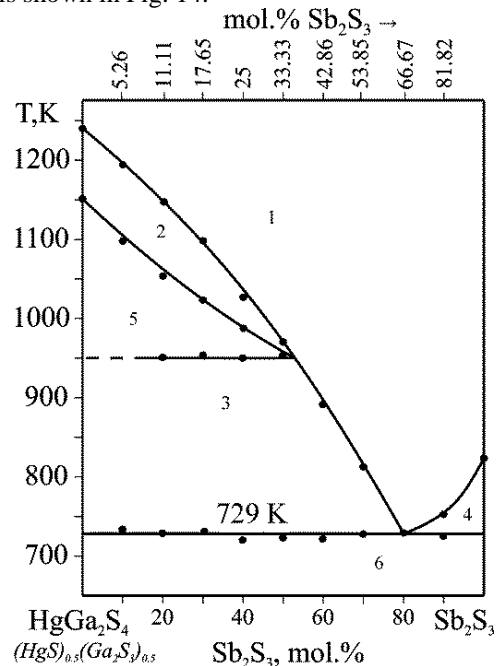
Fig. 14. Phase diagram of the HgGa$_2$S$_4$–Sb$_2$S$_3$ system: 1 – L, 2 – L + HgGa$_6$S$_{10}$, 3 – L + HgGa$_2$S$_4$, 4 – L + Sb$_2$S$_3$; 5 – L + HgGa$_6$S$_{10}$ + HgGa$_2$S$_4$, 6 – HgGa$_2$S$_4$ + Sb$_2$S$_3$. (**Table S5**. Compositions of the alloys of the HgGa$_2$S$_4$–Sb$_2$S$_3$ section re-calculated to the concentration triangle of the quasi-ternary system HgS–Ga$_2$S$_3$– Sb$_2$S$_3$).

The investigated section (Fig.14) belongs to the eutectic type. The vertical section is quasi-binary only in the sub-solidus part due to incongruent mercury thiogallate. Liquidus of the section is described with three fields of the primary crystallization of HgGa$_6$S$_{10}$ (field 2), HgGa$_2$S$_4$ (field 4), and Sb$_2$S$_3$ (field 5). The invariant process at 729 K refers to a binary eutectic L $\leftrightarrow$ HgGa$_2$S$_4$+Sb$_2$S$_3$ which completes the crystallization of all

alloys. The horizontal line at 950 K relates to the peritectic process L + HgGa$_6$S$_{10}$ ↔ HgGa$_2$S$_4$.

2.2.3. The HgGa$_6$S$_{10}$–Sb$_2$S$_3$ section ((HgS)$_{0.2}$(Ga$_2$S$_3$)$_{0.8}$–Sb$_2$S$_3$)

Liquidus of the vertical section HgGa$_6$S$_{10}$–Sb$_2$S$_3$ (Fig.15) consists of three fields of the primary crystallization of β-solid solutions of HT-Ga$_2$S$_3$ (field 2)), β'-solid solutions of LT-Ga$_2$S$_3$ (field 5)), and of Sb$_2$S$_3$ (field 11). The crystallization of all alloys ends in the invariant ternary eutectic process at 680 K L ↔ β'-Ga$_2$S$_3$ + HgGa$_2$S$_4$ + Sb$_2$S$_3$. The horizontal line at 1080 K corresponds to the transition reaction L + β-Ga$_2$S$_3$ ↔ β'-Ga$_2$S$_3$ + HgGa$_6$S$_{10}$. The transition reaction L + HgGa$_6$S$_{10}$ ↔ β'-Ga$_2$S$_3$ + HgGa$_2$S$_4$ takes place at 1003 K leading to the crystallization of mercury thiogallate in the sub-solidus region.
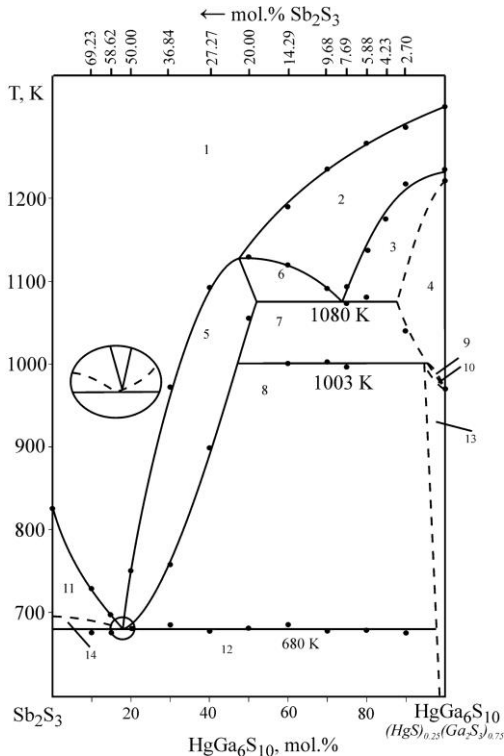

Fig. 15. Phase diagram of the HgGa$_6$S$_{10}$–Sb$_2$S$_3$ system: 1 – L, 2 – L + β-Ga$_2$S$_3$, 3 – L + β-Ga$_2$S$_3$ + HgGa$_6$S$_{10}$, 4 – HgGa$_6$S$_{10}$, 5 – L + β'-Ga$_2$S$_3$, 6 – L + β-Ga$_2$S$_3$ + +β'-Ga$_2$S$_3$, 7 – L + β'-Ga$_2$S$_3$ + HgGa$_6$S$_{10}$, 8 – L + β'-Ga$_2$S$_3$ + HgGa$_2$S$_4$, 9 – β'-Ga$_2$S$_3$ + HgGa$_6$S$_{10}$, 10 – β'-Ga$_2$S$_3$ + HgGa$_6$S$_{10}$ + HgGa$_2$S$_4$, 11 – L + Sb$_2$S$_3$, 12 – β'-Ga$_2$S$_3$ + Sb$_2$S$_3$ + HgGa$_2$S$_4$, 13 – β'-Ga$_2$S$_3$ + HgGa$_2$S$_4$, 14 – Sb$_2$S$_3$ + HgGa$_2$S$_4$, (**Table S6.** Compositions of the alloys of the HgGa$_6$S$_{10}$–Sb$_2$S$_3$ section re-calculated to the concentration triangle of the quasi-ternary system HgS–Ga$_2$S$_3$– Sb$_2$S$_3$).

2.2.4. The HgS–(Ga$_2$S$_3$)$_{0.5}$(Sb$_2$S$_3$)$_{0.5}$

Liquidus of the vertical section HgS–(Ga$_2$S$_3$)$_{0.5}$(Sb$_2$S$_3$)$_{0.5}$ (Fig. 16) consists of four fields of the primary crystallization of β'-Ga$_2$S$_3$ (field 7), HgGa$_6$S$_{10}$ (field 5), HgGa$_2$S$_4$ (field 3), and Sb$_2$S$_3$ (field 2). The crystallization of almost all alloys ends in four-phase eutectic processes L ↔ β'-Ga$_2$S$_3$ + HgGa$_2$S$_4$ + Sb$_2$S$_3$ (680 K) and L ↔ HgS + HgGa$_2$S$_4$ + Sb$_2$S$_3$ (690 K). The

horizontal line at 618 K refers to the polymorphous transformation of mercury sulfide.

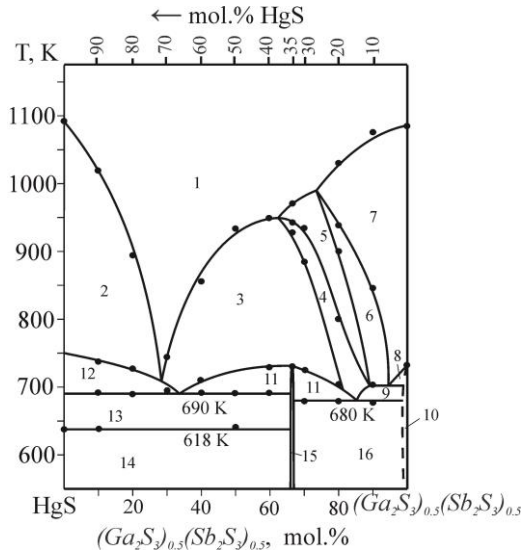**Fig. 16**. Phase diagram of the HgS– (Ga$_2$S$_3$)$_{0.5}$(Sb$_2$S$_3$)$_{0.5}$ system: 1 – L, 2 – L + α-HgS, 3 – L + HgGa$_2$S$_4$, 4 – L + +HgGa$_2$S$_4$ + HgGa$_6$S$_{10}$, 5 – L + HgGa$_6$S$_{10}$, 6 – L + β'-Ga$_2$S$_3$ + HgGa$_6$S$_{10}$, 7 – L + β'-Ga$_2$S$_3$, 8 – L + β'-Ga$_2$S$_3$ + Sb$_2$S$_3$, 9 – L + β'-Ga$_2$S$_3$ + HgGa$_2$S$_4$, 10 – β'-Ga$_2$S$_3$ + Sb$_2$S$_3$, 11 – L + Sb$_2$S$_3$ + HgGa$_2$S$_4$, 12 – L + α-HgS + Sb$_2$S$_3$, 13 – α-HgS + Sb$_2$S$_3$ + HgGa$_2$S$_4$, 14 – δ-HgS + Sb$_2$S$_3$ + HgGa$_2$S$_4$, 15 – HgGa$_2$S$_4$ + Sb$_2$S$_3$, 16 – β'-Ga$_2$S$_3$ + Sb$_2$S$_3$ + HgGa$_2$S$_4$ (**Table S7.** Compositions of the alloys of the HgGa$_6$S$_{10}$–Sb$_2$S$_3$ section re-calculated to the concentration triangle of the quasi-ternary system HgS–Ga$_2$S$_3$– Sb$_2$S$_3$).

2.2.5. Liquidus surface projection of the quasiternary system HgS–Ga$_2$S$_3$–Sb$_2$S$_3$

Phase equilibria in the quasi-ternary system HgS–Ga$_2$S$_3$–Bi$_2$S$_3$ were studied on 82 alloys the chemical and phase composition of which is shown in Fig. 17.

Liquidus surface projection of the HgS–Ga$_2$S$_3$–Sb$_2$S$_3$ is presented in Fig. 17. It consists of six fields of the primary crystallization of α-HgS (field e$_1$E$_1$p$_3$), HgGa$_2$S$_4$ (field p$_3$E$_1$e$_3$E$_2$U$_2$p$_2$), Sb$_2$S$_3$ (field e$_1$E$_1$e$_3$E$_2$e$_2$), HgGa$_6$S$_{10}$ (field p$_2$U$_2$U$_1$p$_1$), β-Ga$_2$S$_3$ (field p$_1$U$_1$m), and β'-Ga$_2$S$_3$ (field mU$_1$U$_2$E$_2$e$_2$) which are separated by ten monovariant lines. The nature and temperature of invariant process are summarized in Fig. 18.

The system HgS–Ga$_2$S$_3$–Sb$_2$S$_3$ is triangulated by the quasi-binary section HgGa$_2$S$_4$– Sb$_2$S$_3$ into two subsystems, HgS–HgGa$_2$S$_4$–Sb$_2$S$_3$ and HgGa$_2$S$_4$–Ga$_2$S$_3$–Sb$_2$S$_3$, that can be considered independently. Crystallization of alloys of the HgS–HgGa$_2$S$_4$–Sb$_2$S$_3$ subsystem is finished in the invariant eutectic process L ↔ α-HgS+Sb$_2$S$_3$+HgGa$_2$S$_4$ at 690 K. Crystallization of alloys in the HgGa$_2$S$_4$–Ga$_2$S$_3$–Sb$_2$S$_3$ subsystem ends in the invariant eutectic process L ↔ β'-Ga$_2$S$_3$+Sb$_2$S$_3$+HgGa$_2$S$_4$ at 680 K.

Taking into account the concentration boundaries and the initial crystallization temperature of mercury thiogallate in the p$_1$E$_1$e$_3$E$_2$P$_2$p$_2$p$_1$ field, such compositions may be proposed in order to grow crystals by solution-melt method: 25 mol.% HgS – 25 mol.% Ga$_2$S$_3$ – 50 mol.% Sb$_2$S$_3$ (T = 900 K), and 50 mol.% HgS – 20 mol.%
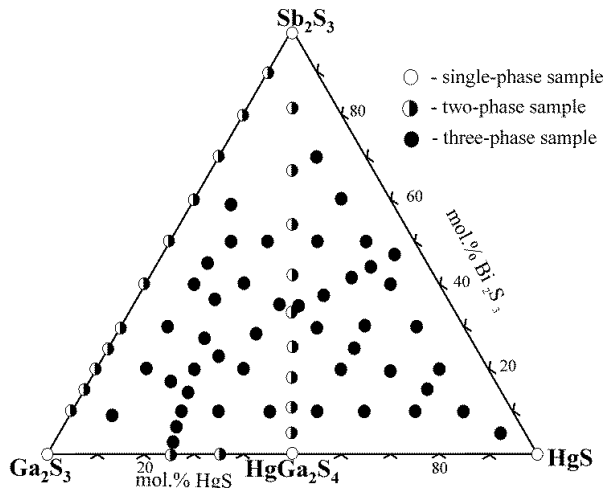
Fig. 17. Chemical and phase composition of the HgS–Ga$_2$S$_3$–Sb$_2$S$_3$ system alloys at 670 K.
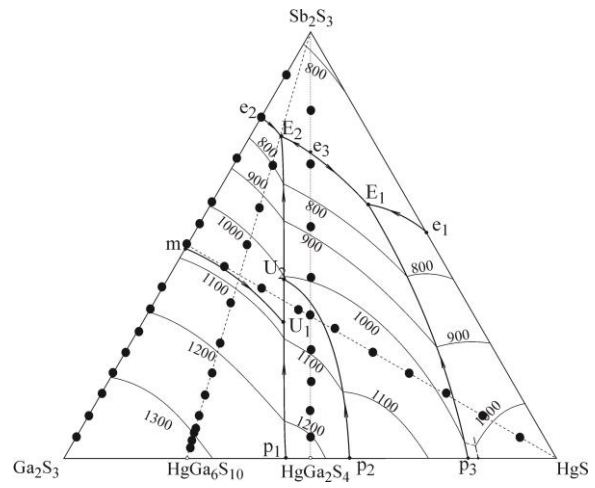

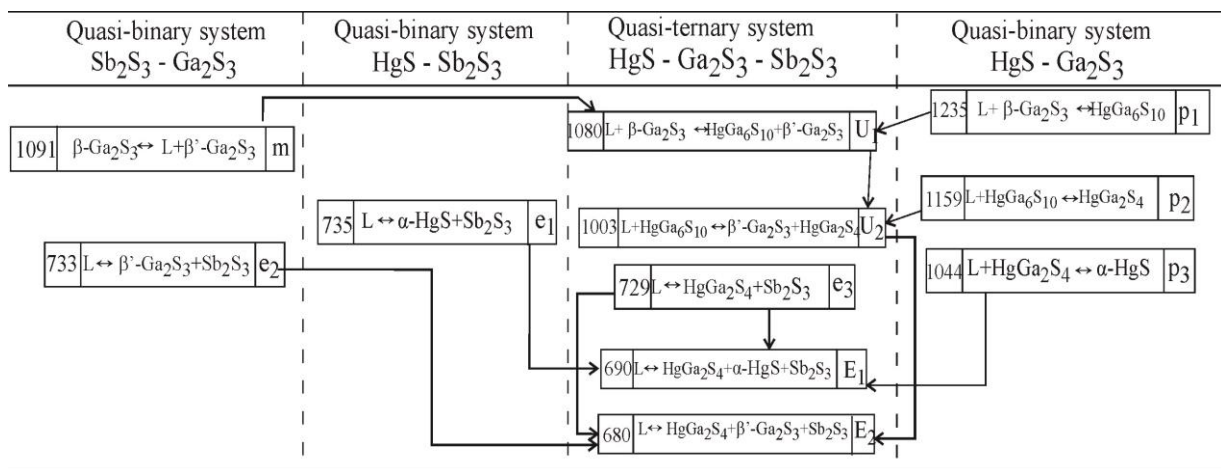**Fig. 18.** Liquidus surface projection of the quasi-ternary system *HgS–Ga$_2$S$_3$–Sb$_2$S$_3$*.

Fig. 19. The nature and temperature of invariant processes in the quasi-ternary system HgS–Ga$_2$S$_3$–Sb$_2$S$_3$

Ga$_2$S$_3$ – 30 mol. % Sb$_2$S$_3$ (T = 1000 K).
The temperature difference between the liquidus and solidus is around 200 K that is a sufficient range for obtaining large single crystals of mercury thiogallate.

Conclusions and Future Work

A total of 177 alloys were investigated by DTA and X-ray diffraction methods in the quasi-ternary systems HgS–Ga$_2$S$_3$–Bi(Sb)$_2$S$_3$.

The liquidus surface projections in the entire concentration range were plotted. Due to large primary crystallization region of mercury thiogallate and low temperature (950-1050 K), the growth of HgGa$_2$S$_4$ single crystals by solution-melt method is possible, particularly at the HgGa$_2$S$_4$–Bi$_2$S$_3$ and HgGa$_2$S$_4$–HgBi$_2$S$_4$ sections. Bi$_2$S$_3$ is favored as a solvent over HgBi$_2$S$_4$ because of smaller amount of HgS involved and, accordingly, a decrease in vapor pressure in a sample of a given composition.

The HgS–Ga$_2$S$_3$–Sb$_2$S$_3$ system also features a large primary crystallization field of mercury thiogallate HgGa$_2$S$_4$. Two compositions were proposed for the single crystal growth by solution-melt method, 25 mol.% HgS – 25 mol.% Ga$_2$S$_3$ – 50 mol.% Sb$_2$S$_3$, and 50 mol.% HgS –

20 mol.% Ga$_2$S$_3$ – 30 mol.% Sb$_2$S$_3$.

Smitiukh O.V. – Ph.D., art. teacher of the Department of Chemistry and Technologies, Volyn National University named after Lesya Ukrainka;

Petrus' I.I. – Ph.D., researcher of the Department of Chemistry and Technologies, Volyn National University named after Lesya Ukrainka.

[1] M. V. Kabanov, Yu. M. Andreev, V. V. Badikov, and P. P. Geiko, *Parametric frequency converters based on new nonlinear crystals*, Russ. Phys. J., 46(8). 835 (2003); https://doi.org/10.1023/B:RUPJ.0000010980.77569.84.

[2] R. Nitsche, H. U. Bölsterli and M. Lichtensteiger, *Crystal growth by chemical transport reactions - Binary, ternary, and mixed-crystal chalcogenides*, J. Phys. Chem. Solids. 21(3-4), 199 (1961); https://doi.org/10.1016/0022-3697(61)90098-1.

[3] P.G. Schunemann, T.M. Pollak, *Synthesis and Growth of HgGa$_2$S$_4$ crystals*, J. Crystal growth. 174, 278 (1997); https://doi.org/10.1016/S0022-0248(96)01158-X.

[4] R. C. Sharma, Y. J. L Chang, C. Guminski, The Hg-S (mercury-sulfur) system, JPE, 14(1), 100 (1993);. https://doi.org/10.1007/bf02652168.

[5] A. Zavrazhnov, S. Berezin, A. Kosykov, et al. *The phase diagram of the Ga–S system in the concentration range of 48.0–60.7 mol% S,.* J. Therm. Anal. Calorim,.. 134, 483 (2018); https://doi.org/10.1007/s10973-018-7124-z.

[6] J.C. Lin, R.C. Sharma, & Y.A. Chang, *The Bi-S (Bismuth-Sulfur) system*. JPE. 17. p 132 (1996.); https://doi.org/10.1007/BF02665790.

[7] N.Kh. Abrykosov, V.F. Bankyna, L.V. Poretskaia, y dr. Poluprovodnykovye khalkohenidy i splavy na ikh osnove, *Moscow: Nauka* 1975. 173 pages (*In Russian*).

[8] State Diagrams of Binary Metallic Systems: *Handbook*: M.: Mashinostroenie (edited by Lyakisheva N.P.), 1996. 1. 992 pages.

[9] P. Bayliss, W. Nowacki, *Refinement of the crystal structure of stibnite, Sb$_2$S$_3$*. ZEKGA, 135. p 308 (1972.); https://doi.org/10.1524/zkri.1972.135.16.308.

[10] Scavnicar S. Stibnite. *A redetermination of atomic positions*. Z.Kristall. 114, 85 (1960.); https://doi.org/10.1524/zkri.1960.114.16.85.

[11] W.G. Mumme, J.A. Watts, *HgBi$_2$S$_4$: Crystal structure and relationship with the pavonite homologous series*. Acta Cryst., B 36, 1300 (1980.); https://doi.org/10.1107/S0567740880005973.

[12] H. Schwer, V.Kraemer, *The crystal structures of CdAl$_2$S$_4$, HgAl$_2$S$_4$, and HgGa$_2$S$_4$*. Z.Kristall. 190, 103 (1990); https://doi.org/10.1524/zkri.1989.190.14.103

[13] Števko Martin, Sejkora, Jiří, and Peterec Dušan. *Grumiplucite from the rudňany deposit, Slovakia: A second world-occurrence and new data,* Journal of Geosciences (Czech Republic), 60 (4). P. 269 (2015); https://doi.org/10.3190/jgeosci.200.

[14] Alsulami Abdullah, Al-Zahrani H.Y.S., *Optical characteristics of chemically deposited MnSb$_2$S$_4$ thin films*. Physica B: Condensed Matter, 657. Article number 414786 (2023); https://doi.org/10.1016/j.physb.2023.414786.

[15] Rahnamaye H.A. Aliabad, M. Mousavi, A. Abareshi, *First-principles calculations of optoelectronic and thermoelectric properties of HgGa$_2$S$_4$ chalcopyrite under pressure effect*, Materials Science and Engineering: B. 272, 115336 (2021.).

[16] I.A. Zharikov, V.Yu. Rud, Yu.V. Rud, V.V. Davydov, N.N. Bykova, *Photosensitivity of structures based on $A^{II}B^{III}_2C^{VI}_4$ monocrystals*, Journal of Physics: Conference Series. 1038(1). 012100 (2018).

[17] I. D. Olekseyuk, I. I. Mazurets, O. V. Parasyuk, *Phase equilibria in the HgS–Ga$_2$S$_3$–GeS$_2$ system*, Journal of Alloys and Compounds. 417(1-2). p 131 (2006); https://doi.org/10.1016/j.jallcom.2005.09.036.

[18] N. A. Il'yasheva, E. F. Sinyakova, B. G. Nenashev, and I. V. Sinyakov. Izv. Akad. Nauk SSSR, Neorg. Mater. 2**1**(11) 1860 (1985), Neorg. Mater. Engl. Transl. 21, 1618 (1985).

[19] M.B. Babanly, A.A. Kurbanov, A.A. Kuliev, *Phase equilibria and intermolecular interaction in the HgS–Sb$_2$S$_3$(Bi$_2$S$_3$) systems. Izv. AN SSSR*, *Inorgan.Materials*. 16(3). p 547 (1980).

[20] W. S. Brower, H. S. Parker, R. S. Roth, *Synthesis of mercury bismuth sulfide HgBi$_2$S$_4$*, Mater. Res. Bull. 1973. 8, 859 (1973);); https://doi.org/10.1016/0025-5408(73)90193-1.

[21] M. Guittard, M.-P, Pardo, C. Ecrepont, *Phase diagram of the system Bi$_2$S$_3$-Ga$_2$S$_3$*. C.R.Acad. Sci. Paris. 307, 141 (1988).

[22] S. Barnier, M. Guittard, C. Julien and A. Chilouet, *Etude de l'environnement de l'antimoine dans les verres gallium-antimoine-soufre en liaison avec le diagramme de Phase et les spectres d'absorption infrarouge Study of the antimony environment in gallium-antimony-sulphur glasses - Phase diagram and infrared absorption investigations*. Mater. Res. Bull. 28 (5), 399 (1993).

[23] L. Akselrud, and Yu. Grin, *WinCSD: Software Package for Crystallographic Calculations (Version 4),* J. Appl. Cryst, 47, 803 (2014); https://doi.org/10.1107/S1600576714001058.

O.V. Smitiukh, I.I. Petrus'

О.В. Смітюх, І.І. Петрусь

Фазові рівноваги в системах HgS–Ga$_2$S$_3$–Bi(Sb)$_2$S$_3$

Волинський національний університет імені Лесі Українки, кафедра хімії та технології, м. Луцьк, Україна,
Smitiukh.Oleksandr@vnu.edu.ua

Фазові рівноваги в квазіпотрійних системах HgS–Ga$_2$S$_3$–Bi(Sb)$_2$S$_3$ були досліджені із використанням фізико-хімічних методів аналізу 177 сплавів, які були синтезовані одно температурним методом. У роботі представлено фазові рівноваги квазібінарних систем HgS–Bi$_2$S$_3$ і Ga$_2$S$_3$–Bi$_2$S$_3$, шести перерізів (HgGa$_2$S$_4$–HgBi$_2$S$_4$, HgGa$_2$S$_4$–Bi$_2$S$_3$, HgGa$_6$S$_{10}$–Bi$_2$S$_3$, HgGa$_6$S$_{10}$–HgBi$_2$S$_4$, HgGa$_2$S$_4$–Sb$_2$S$_3$, and HgS–"GaSbS$_3$") і поверхня ліквідусу досліджених систем. Встановлено, що в системах існує велика область первинної кристалізації тіогалату, зокрема на перерізах HgGa$_2$S$_4$–Bi$_2$S$_3$ і HgGa$_2$S$_4$–HgBi$_2$S$_4$, і низька температура плавлення (950-1050 K). Тому, як зручний метод вирощування монокристалів тіогалату пропонуємо використовувати розчин-розплавний метод.

Ключові слова: фазові діаграми, солідус, квазібінарна система, поверхня ліквідусу системи.